Open Access Library Journal
2026, Volume 13, e15316
ISSN Online: 2333-9721
ISSN Print: 2333-9705

Hydro-Mechanical Response and Damage Mechanisms of Geosynthetic-Reinforced Slopes under Rainfall Infiltration: An Integrated Experimental and FLAC3D Numerical Study

Chatowa Chembe

College of Environment and Civil Engineering, Chengdu University of Technology, Chengdu, China
Email: chatowachembe@gmail.com

How to cite this paper: Chembe, C. (2026) Hydro-Mechanical Response and Damage Mechanisms of Geosynthetic-Reinforced Slopes under Rainfall Infiltration: An Integrated Experimental and FLAC3D Numerical Study. *Open Access Library Journal*, **13**: e15316.
https://doi.org/10.4236/oalib.1115316

Received: April 9, 2026
Accepted: June 13, 2026
Published: June 16, 2026

Abstract

Slope failures due to rainfall are one of the main factors that cause damage to transportation infrastructures, embankments, and earth structures even with reinforcement in the tropical and sub-tropical areas. This paper uses combined experimental and numerical methods to study the hydro-mechanical behavior of geosynthetic reinforced slopes as well as the morphing of the damage process as a result of rainfall infiltration. The new research method is making use of instrumented rainfall flume bench-scale experiments coupled with hydro-mechanical advanced simulations done with the software FLAC3D for an in-depth evaluation of transient pore-water pressure changes, matric suction reductions, slope deformation as well as reinforcement loading under different rainfall intensities. High-tech monitoring techniques such as tensiometers, pore-water pressure transducers, TDR moisture probes, strain gauges, and laser displacement sensors were deployed to the experimental program. All of these were combined to trace the coupled hydraulic and mechanical response of a partially saturated reinforced slope under rainfall infiltration. Variably saturated flow using Richards' equation, soil-water characteristic curves using van Genuchten relationship, effective stress concept using Bishop's formulation, and Mohr-Coulomb constitutive model were numerically simulated to replicate infiltration-led failure phenomena. The findings illustrated that rainfall intensities remained the primary factor controlling degradation and stability loss through hydro-mechanical interaction. Heavy rainfall brought about very quick positive pore-water pressure build-up, facilitated fast loss of matric suction and favored the formation of localized saturation zones next to the interface of the reinforcement layers. These were the main causes of the significant rise in reinforcement thrust and deformation build-up. When put against low-intensity

rainfall scenarios, high-intensity admission caused reinforcement thrust to increase by roughly 175% and the factor of safety was downgraded from stable to near-failure levels. Parametric studies disclosed that drainage systems markedly raise the performance of reinforced slopes by controlling pore-pressure build-up and hastening post-rainfall dissipation. The FLAC3D modeling platform validated against the experimental data demonstrated an excellent match with the experimental results and thereby served as a powerful tool for performance-based design evaluation under short-term rainfall occurrences. Besides, the research presented fruitful design guidelines and stability maps that relate rainfall intensity, duration, reinforcement arrangement, and drainage features to slope performance. These results greatly help in understanding the hydro-mechanical coupling processes in reinforced slopes and therefore constitute a useful reference for designing climate-resilient geotechnical infrastructures facing increasing rainfall extremes due to climate change.

Subject Areas

Geotechnical Engineering

Keywords

Rainfall Infiltration, Geosynthetic-Reinforced Slopes, Unsaturated Soil, Hydro-Mechanical Coupling, FLAC3D, Pore-Water Pressure, Matric Suction, Slope Stability, Numerical Simulation, Reinforcement Interaction

1. Introduction

Instability of slopes due to rainfall-triggered landslides remains one of the most critical and recurring problems in geotechnical engineering, especially in tropical and monsoon areas that are exposed to prolonged and heavy rains. Both natural and engineered slope failures due to rainfall infiltration have resulted in damaged infrastructures, economic loss, and loss of lives all over the world. The main triggering factor is related to complicated hydro-mechanical interactions in partially saturated soils, where infiltration into soil leads to in-situ stress state changes since matric suction is lowered and thus, the degradation of the soil shear strength occurs [1] [2].

The hydro-mechanical behavior of unsaturated soils undergoing rainwater infiltration can be effectively modeled by employing Bishop's effective stress concept [3]:

$$\sigma' = (\sigma - u_a) + \chi(u_a - u_w)$$

where σ' is the effective stress, σ is the total stress, u_a is the pore-air pressure, uw is the pore-water pressure, and χ is the effective stress parameter related to the degree of saturation. The difference $(u_a - u_w)$ is called matric suction, which plays a very important role in giving partially saturated soils apparent cohesion and shear strength. When rainwater infiltrates the soil, the wetting front

moves downward into the slope, increasing the degree of saturation and making the soil less dry, that is, reducing matric suction. As a result, the apparent cohesion diminishes leading to a stepwise decline in slope safety and factor of safety.

Geosynthetic-Reinforced Soil (GRS) is an innovative technique that has a lot of potentials in infrastructure facilities, fill embankments, and retaining walls due to its low cost, ease of construction, and tolerance of high deformations. However, there is still some uncertainty regarding how these structures will behave when exposed to permeating water and rainfall. Traditional methods of assessing the stability of slopes often continue to overlook this dynamic scenario of unsaturated soil-water interaction characterizing real rainfalls [4] [5].

In the past couple of years, there have been quite a few reports about reinforced soil slopes damaged during the typhoon and monsoon seasons in Southeast Asia. Such failures have been linked to the build-up of positive pore-water pressures in the low permeable backfills. These pressure increments generally cause large deformations, excessive loading of reinforcements, and finally structural failure [6]. Events like these make it clear to us that using hydro-mechanical coupled analyses is very important, which will help us to better simulate the infiltration behavior, time changes of pore pressure, and reinforcement loadings under different rainfalls.

The socio-economic costs of landslides triggered by rainfall are huge. Everywhere that landslides happen, they not only disrupt road networks but also endanger houses and other structures and, above all, result in quite a number of casualties. According to global landslide records, the main cause of landslides in tropical and subtropical areas is heavy rain (about 90%) [7]. Besides, the forecast changes of climate are that there will be more and more rainfall of very high intensities, thus, landslide danger, in particular, of reinforced slopes will be on the rise keeping us in need of more resilient and performance-based design of such slopes with the ability to withstand extreme climatic conditions.

This paper conducted thorough laboratory experiments and numerical modeling of the hydro-mechanical behavior and failure mechanisms of geosynthetic-reinforced slopes under the influence of rainfall infiltration. Pore-water pressure, matric suction, displacement, and reinforcement stress have been studied with a number of instrumented rainfall flume experiments supported by advanced numerical modeling in FLAC3D. Bishop's effective stress concept, van Genuchten soil-water retention relation and Mohr-Coulomb soil model were implemented in the numerical model to describe the coupled behavior of reinforced soil with partial saturation. These results are in line with the validated computational framework which is of immense help in design for performance of reinforced slopes through extreme weather scenarios.

2. Literature Review

2.1. Fundamental Principles of Unsaturated Slope Behavior

The theoretical framework governing unsaturated slope behavior has evolved sub-

stantially following the foundational contributions of Bishop [3] and Fredlund [1]. These pioneering studies established that matric suction contributes significantly to the shear strength of partially saturated soils by generating apparent cohesion. Unlike fully saturated soils, unsaturated geomaterials exhibit coupled hydraulic and mechanical behavior in which pore-air and pore-water pressures simultaneously influence effective stress and deformation response.

The shear strength of unsaturated soils can be represented using the extended Mohr-Coulomb failure criterion:

$$\tau_f = c' + (\sigma_n - u_a)\tan\phi' + (u_a - u_w)\tan\phi_b$$

where τ_f represents shear strength, c' denotes effective cohesion, σ_n is the normal stress, u_a is pore-air pressure, u_w is pore-water pressure, and ϕ_b represents the angle describing the rate of increase in shear strength with matric suction. The term $(u_a - u_w)$ corresponds to matric suction, which contributes additional shear resistance in unsaturated conditions.

A critical relationship governing unsaturated soil behavior is the Soil-Water Characteristic Curve (SWCC), which links matric suction to water content and degree of saturation. Among various formulations, the van Guchten model [8] remains the most widely adopted because of its robustness and computational efficiency:

$$\Theta = \frac{\theta - \theta_r}{\theta_s - \theta_r} = \left[1 + (\alpha\psi)^n\right]^{-m}$$

Here, Θ is the effective saturation, θ the volumetric water content, θ_r and θ_s are the residual and saturated volumetric water contents, ψ is the matric suction, while empirical fitting parameters α, n, and m control the shape of the retention curve. The soil-water characteristic curve (SWCC) describes the infiltration behavior, the evolution of permeability, and the dissipation of suction during rainfalls; thus, it strongly influences the hydro-mechanical slope analysis.

2.2. Laboratory Testing on Rainfall-Induced Landslides

Physical modeling with the help of rainfall flume experiments has been a major contributor to the knowledge of infiltration mechanisms and rainfall-triggered landslide failures. Large-scale flume experiments by Chengdu University of Technology, and the Institute of Mountain Hazards and Environment among others have yielded excellent sets of data describing the transient hydro-mechanical behavior under controlled rainfall conditions [9].

These experiments are usually equipped with a sophisticated set of instrumentation systems, including tensiometers, pore-water pressure transducers, TDR moisture probes, optical displacement tracking systems, and strain gauges embedded within reinforcement layers. Such instrumentation offers the possibility of high-resolution monitoring of suction variation, moisture migration, displacement evolution, and reinforcement loading during rainfall infiltration.

Li *et al.* [9] conducted extensive flume tests on bedded rock slopes containing

weak interlayers and found that preferential flow along discontinuities drastically speeds up infiltration and resulting instability development. According to their results, geological structures are a strong determinant of failure mechanisms since they control localized pore-pressure build-up and seepage paths. In a similar vein, He and Wang [10] employed photogrammetric monitoring methods to document deformation fields during progressive slope failure, and collected high-quality datasets suitable for validating coupled numerical models.

Around the world, Josifovski *et al.* [11] performed carefully instrumented experiments on unsaturated sandy slopes subjected to rainfall infiltration. Their work led to the development of reference datasets for pore-pressure evolution and displacement histories and illustrated the extreme nonlinearity between rainfall intensity and slope deformation response. Their results revealed critical rainfall thresholds, beyond which progressive failure processes are triggered very quickly.

2.3. Latest Developments in Numerical Modeling of Coupled Hydro-Mechanical Processes

With the advent of new constitutive models, improved computational algorithms, and enhanced computer performance, there have been quite significant advances in numerical simulation methods for coupled hydro-mechanical slope analysis. Previously, analytical methods were often based on simplified infiltration approximations and combined with ordinary limit-equilibrium methods. While these methods were computationally efficient, they fell short in accurately capturing transient pore-pressure variations and their interaction with soil reinforcement systems [12].

More and more geotechnical engineering practices are turning to complete coupled finite element and finite difference methods which are able to simultaneously calculate the hydraulic and mechanical fields equations. D'Alessio *et al.* [13] introduced a full FLAC3D scheme for analyzing the stability of embankments under rainfall infiltration and verified their numerical forecasts with the field monitoring data. The work of the authors has set up reliable methods for the calibration of the van Genuchten hydraulic parameters and has shown that coupled analysis gives much better results than traditional uncoupled methods.

As far as the systems of reinforced slopes are concerned, Yang *et al.* [6] have put forward one of the biggest ones that involved a coupled hydro-mechanical numerical modeling of a multi-tier geosynthetic-reinforced slope exposed to the typhoon rainfall. Their post-mortem investigation has shown that the accumulation of the positive pore-water pressure within the low-permeability materials of the backfill has essentially changed the mechanism of the slope failure, and has led to the development of the compound slip surfaces which were untraceable accurately by conventional design methods.

More recently, Kumar *et al.* [14] have stressed the necessity of incorporating the climate change scenarios in the slope stability analysis. Their outcomes show that the current design rainfall events may largely underestimate the risk of future

failure in tropical regions that will be getting more and more rainfall-intense due to the climate change.

2.4. The Influence of Vegetation on Slope Stability

Recently, there has been a growing emphasis on the role of vegetation in slope stability due to its joint hydrological and mechanical effects. Besides mechanically reinforcing the slope by roots, vegetation also affects the infiltration by modifying the evapotranspiration and suction retention.

Sadeghi *et al.* [15] revealed, from coupled hydro-mechanical simulations, that vegetated slopes retain considerably higher safety factors than bare slopes when subjected to the same rainfall conditions. Their results were mainly based on the higher matric suction that kept being retained and the extra reinforcement through the root network. Similarly, Fata *et al.* [16] measured the hydrological and mechanical actions of vegetation on the prevention of landslides and it was found that the choice of the right vegetation species and planting densities have a major impact on the resistance to rainfall-induced instability.

The incorporation of vegetation effects within hydro-mechanical numerical frameworks is a necessary step towards the development of sustainable and climate-resilient slope stabilization methods.

2.5. Unsolved Research

Although experimental and numerical researches on rainfall-induced slope instabilities have been dramatically ramped up, there is still a number of key research gaps that need to be filled. First, there is a shortage of instrumented rainfall experiments on reinforced slopes which are able to simultaneously measure reinforcement thrust, matric suction, pore-pressure response, and displacement evolution with high temporal resolution.

Second, there is not a lot of literature to show that reinforcement layout, drainage conditions, rainfall intensity, and soil hydraulic properties have been thoroughly studied together through parametric analysis.

Third, there is a lack of open and reproducible hydro-mechanical modeling workflows for unsaturated reinforced slopes that can serve as benchmarks and validation tools for different investigations.

Moreover, the level of understanding of soil-reinforcement interface behavior under transient saturation conditions is still insufficient, especially with regard to the degradation of interface shear resistance during infiltration. Lastly, vegetation effects are still poorly incorporated within coupled hydro-mechanical frameworks for reinforced slope systems.

2.6. Objectives of Research and Delimitation of the Study

To close the existing research gaps, this research will carry out an integrated experimental and numerical study on the hydro-mechanical behavior of geosynthetic reinforced slopes subjected to rainfall infiltration. Research objectives in-

clude:

- To design and conduct controlled instrumented rainfall flume experiments on geosynthetic-reinforced slopes under varying rainfall intensities and durations in order to capture detailed hydro-mechanical response data.
- To develop, calibrate, and validate a coupled hydro-mechanical numerical model in FLAC3D capable of reproducing experimentally observed infiltration behavior, deformation response, and soil-reinforcement interaction.
- To perform comprehensive parametric analyses investigating the effects of rainfall characteristics, reinforcement layout, drainage capacity, and soil hydraulic properties on slope stability and deformation behavior.
- To synthesize the numerical and experimental findings into practical design guidance, including stability charts and performance-based recommendations for reinforced slope systems subjected to rainfall infiltration.

The work described in this thesis covers experimental design and instrumentation, numerical modeling, and application to engineering. The basilar point in the continuum is the pivotal transition from the unsaturated to saturated condition and its direct influence on pore-pressure generation, reinforcement loading, and progressive failure development in reinforced slopes.

3. Experimental Program Design

3.1. Soil Characterization and Hydraulic Properties

The soil employed for the experiments was a poorly graded sand with 15% silt that was chosen to be a typical reinforced backfill material with the possibility of carefully controlled unsaturated hydraulic behavior. Thorough laboratory characterization including the determination of hydraulic and shear strength properties that are most relevant to rainfall infiltration response, was carried out in conformity with ASTM standards.

Particle-size distribution was analyzed by using sieve and hydrometer tests which resulted in the following: median particle size (D50) = 0.3 mm, coefficient of uniformity (Cu) = 4.2, and coefficient of curvature (Cc) = 1.1. Standard Proctor compaction tests revealed a maximum dry density of 17.2 kN/m^3 at optimum moisture content of 12%. Direct shear testing under saturated condition was used to establish the effective shear strength parameters, which were effective cohesion, $c' = 1$ kPa and effective friction angle, $\phi' = 32^\circ$.

In order to get the Soil-Water Characteristic Curve (SWCC) over a broad range of suction, unsaturated hydraulic profiling of the soil was realized through both pressure plate extractor and hanging column methods. Experimental data showed a perfect match to the van Genuchten model [8], and the resulted parameters obtained through fitting were $\alpha = 0.8$ kPa^{-1}, $n = 2.5$, $m = 0.6$, $\theta_s = 0.38$, and $\theta_r = 0.08$, which are in line with those reported in related studies [8] [13]. Finally, hydraulic conductivity functions that were derived using Mualem's method forecasted a saturated hydraulic conductivity of $k_{sat} = 5 \times 10^{-5}$ m/s, and also characteristic permeability decline under dry soil conditions.

$$\Theta = \frac{\theta - \theta_r}{\theta_s - \theta_r} = \left[1 + (\alpha\psi)^n\right]^{-m}$$

where Θ represents effective saturation, θ is volumetric water content, θ_r and θ_s denote residual and saturated volumetric water contents, ψ is matric suction, and α, n, and m are fitting parameters governing the shape of the SWCC relationship (see Table 1).

Table 1. Comprehensive soil properties.

Property	Value	Unit	Test Standard
Specific Gravity, Gs	2.65	–	ASTM D854
Maximum Dry Density		kN/m^3	ASTM D698
Optimum Water Content	12	%	ASTM D698
Effective Cohesion, c'	1	kPa	ASTM D3080
Effective Friction Angle, ϕ'	32	°	ASTM D3080
Saturated Hydraulic Conductivity	5×10^{-5}	m/s	ASTM D5084
van Genuchten α	0.8	kPa^{-1}	Fitted
van Genuchten n	2.5	–	Fitted
Residual Volumetric Water Content	0.08	–	Fitted
Saturated Volumetric Water Content	0.38	–	Fitted

3.2. Model Slope Construction and Instrumentation

A steel framework encased the physical model of the slope and served as a rigid flume. It had the following interior measurements: 2.0 m length, 0.5 m width, and 1.0 m height. The front wall was made of a clear polycarbonate panel that allowed both visual observation of the changes occurring and laser-optical detection of the movements during the infiltration of rainfall.

Model slope shapes featured an inclination of 1V:2H which approximately corresponded to a slope angle of 26.6˚. At the same time, the total height of the slope was 0.8 m and its width at the top was 0.4 m. The reason for the choice of this shape was the possibility to realistically represent the behavior of the slope while still being compatible with the constraints of the lab setting.

Soil was laid by moist tamping and compacted in 50 mm layers to reach a dry density of 16.5 kN/m^3 which corresponded to 95% relative compaction. Besides, the initial water content was set at 10%, so the initial degree of saturation was roughly 45%. Thus, they were intended to represent field compaction states typically found in partially saturated reinforced embankments where matric suction is accounted for being a major component of shear strength. Besides, the chosen conditions are consistent with works of Li *et al.* [9] and He and Wang [10].

One reinforcement that was a woven geotextile fabric with pretty high stiffness in the axial direction J = 500 kN/m, was installed at the middle level of the slope, 0.4 m above the bottom. The reinforcement was taken beyond the slope face 1.4

m so as to ensure full activation of the interface resistance and tensile load transfer during rainfall-induced deformation.

The whole system of instruments was set up to keep track of both hydraulic and mechanical changes during the tests. Moreover, the monitoring set-up comprised six tensiometers (UMS T5) to measure suction; four miniature pore-water pressure transducers (GE Druck PDCR81), eight TDR moisture probes (Campbell Scientific CS655), twelve strain gauges (Vishay CEA-06-250UW-350) grappling with the reinforcement layer, and two laser displacement sensors (Keyence IL-300) combined with digital image correlation techniques for deformation tracking. All instruments were linked to a centralized data acquisition system (National Instruments cDAQ-9188) that was running at a sampling frequency of 1 Hz (see Figure 1).

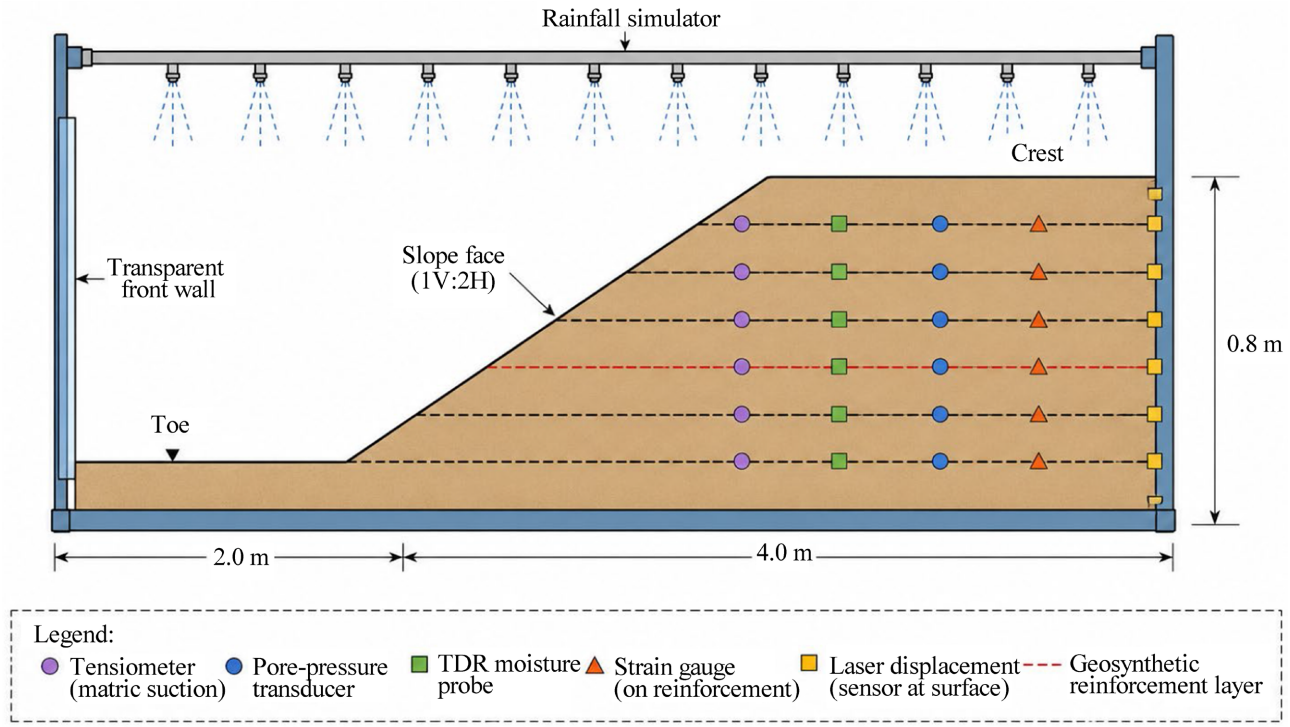

Notes:
1.Five reinforcement layers are installed at vertical spacing of 0.15-0.20 m.
2. Sensors are arranged at different locations to capture hydrological and mechanical responses.

Figure 1. Schematic illustration of the instrumented rainfall flume setup showing slope geometry, reinforcement layout, and sensor arrangement.

3.3. Rainfall Simulation and Testing Protocol

Rainfall infiltration was mimicked with a pressurized nozzle rainfall system. This system was furnished with computer-controlled solenoid valves that could generate rainfall intensities in the range of 2 to 100 mm/h. The rainfall simulator was capable of achieving a spatial uniformity coefficient of over 85%. Calibration steps were taken based on the measurements of the spatial rainfall distribution and characterization of droplet size to make sure that the infiltration conditions were

representative of natural rainfall events.

The experimental program comprised six main rainfall scenarios:

1. No rainfall applied, post preparation only.
2. Light intensity rainfall of 5 mm/h applied for 10 h, resulting in a total rainfall of 50 mm.
3. Heavy intensity rainfall of 25 mm/h applied for 2 h, resulting in a total rainfall of 50 mm.
4. Very heavy intensity rainfall of 50 mm/h applied for 1 h, resulting in a total rainfall of 50 mm.
5. Multi-stage rainfall event imitating the natural variability of rainfall intensities during a synoptic storm.
6. Variation of drainage scenario identical to the heavy rainfall but with improved basal drainage conditions.

Continuous recording of the responses was kept not only during the rainfall but also throughout the 24 hours after the rainfall ceased. Besides the post-test parts included the determination of moisture content, review of reinforcement and mapping of failure surface as per the guidelines of Josifovski *et al.* [11].

To ensure reproducibility and reliability of the experiments, each rainfall scenario was conducted three times under exactly the same boundary and loading conditions. After each rainfall experiment, the model slope was rebuilt using the same moist tamping and compaction methods. Soil moisture content and dry density were carefully checked before each test to make sure that the initial matric suction and saturation conditions were consistent.

Before installation, all monitoring instruments were calibrated as per manufacturer specifications. Besides, during the experimental program experience, further calibration checks were made at regular intervals to limit the influence of the drift of measurements and systematic errors. The analysis of repeatability showed that the variations in measured pore-water pressure, displacement and moisture response remained within ±5% among repeated tests, thereby confirming good experimental reliability (see Table 2 and Figure 2).

Table 2. Experimental rainfall test matrix.

Test Scenario	Rainfall Intensity (mm/h)	Duration (h)	Total Rainfall (mm)	Drainage Condition
Initial Condition	0	0	0	Standard
Low-Intensity Rainfall	5	10	50	Standard
High-Intensity Rainfall	25	2	50	Standard
Extreme Rainfall	50	1	50	Standard
Multi-Stage Rainfall	Variable	Variable	Variable	Standard
Drainage Variant Test	25	2	50	Enhanced Drainage

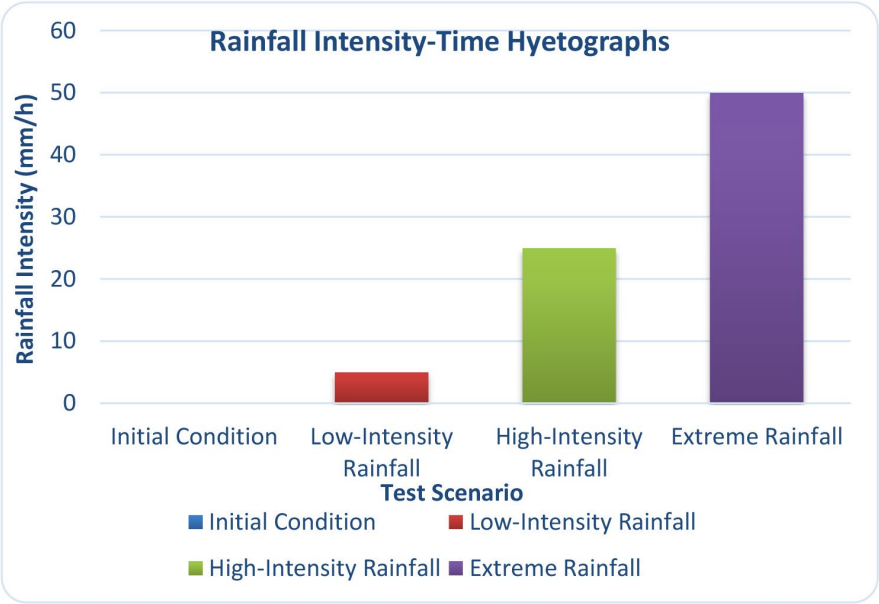

Figure 2. Rainfall intensity-time hyetographs adopted for the experimental testing program.

3.4. Extreme Rainfall and Drainage Variant Tests

Using a rainfall intensity of 50 mm/h, the extreme-intensity rainfall test, out of all the scenarios, produced the hydro-mechanical response at the highest level. However, excessive rainfall absorption by the soil caused the pore-water pressure to be positive, and after only about 20 minutes of rainfall, these pressures peaked at around 3.8 kPa right at the reinforcement level. Besides infiltration, the surface of the ground was covered by water in many places and there were some local saturation spots that led to significant slope deformations mostly near the slope toe and the reinforcement boundary.

The displacement at the crest reached more than 30 mm, the compound failure mechanism was with the involvement of surface sliding and deeper rotational movement. Moreover, the fact that post-rainfall drainage took more than 32 hours, undoubtedly showed the poor state of dissipation of the slope in extreme rainfall situations.

A multi-rainfall-stages scenario effects associated with the repeated wetting and partial drainage cycles were shown. Drainage between intermediate intervals could temporarily lower pore-water pressure, but the addition of repeated rainfall pulses would lead to a decrease in matric suction and an increase in residual saturation within the slope mass. Therefore, delayed acceleration in deformation appeared during the last rainfall stages, a clear indication that antecedent moisture conditions play a significant role in the performance of reinforced slopes.

Regarding the drainage variant test, drastically better results were obtained in relation to the high-intensity rainfall scenario without the provision of enhanced drainage. Basal drainage adequately brought down the development rate of peak pore-water pressure, made the dissipation after rainfall faster, and curtailed the

accumulation of deformation during the entire testing time. Maximum displacement was reduced by almost 40%, and the reinforcement strain was still more or less evenly spread along the length of the reinforcement. This is further evidence of the fact that drainage systems are a major factor in the prevention of rainfall-induced instability in reinforced slopes.

Also, additional experimental scenarios revealed that very high rainfall combined with a lack of proper drainage conditions can lead to rather quick hydro-mechanical degradation, while the use of improved drainage systems on the other hand mitigates pore-pressure build-up and results in better overall slope stability during transient infiltration events (see Figure 3).

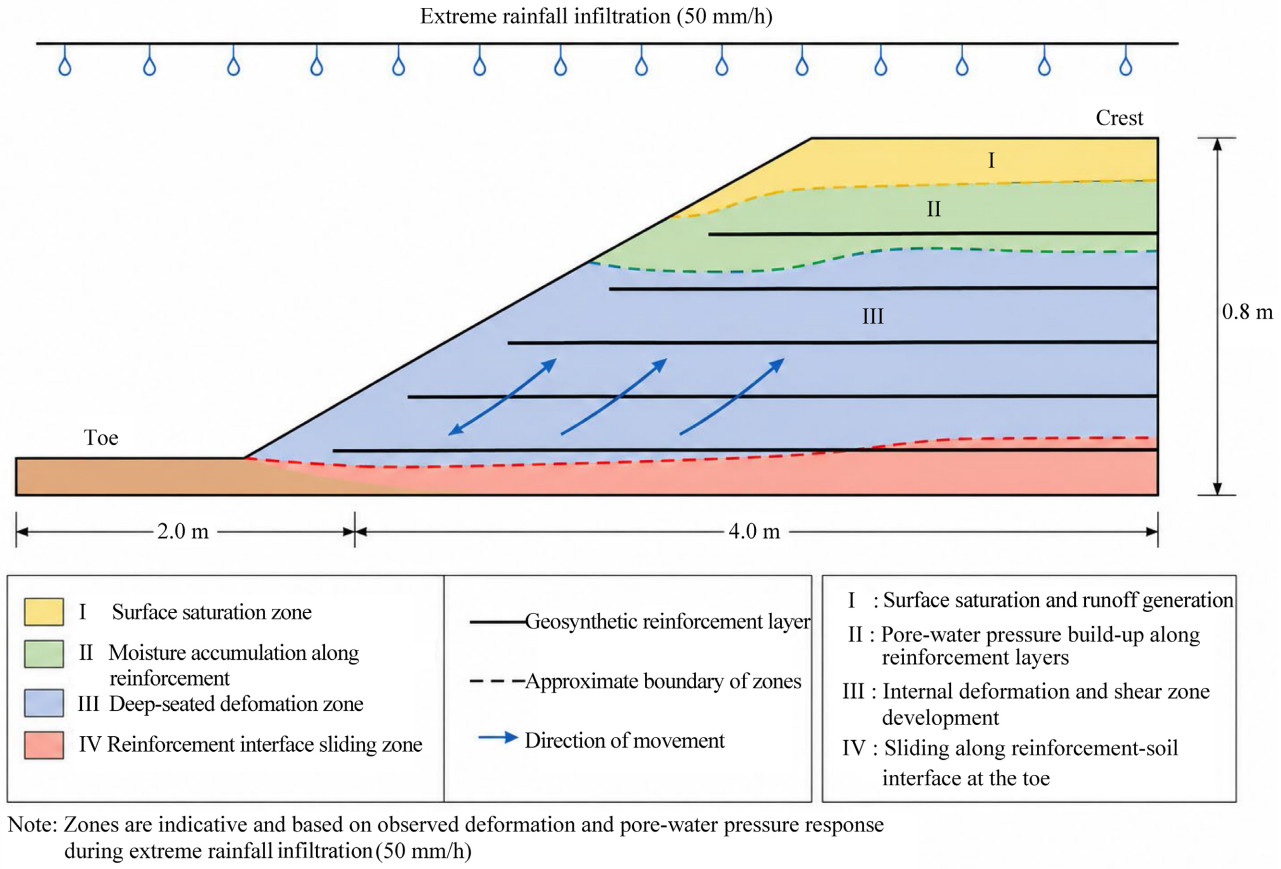

Figure 3. Zones of deformation and failure resulting from extreme rainfall infiltration conditions.

4. Numerical Modeling Framework

4.1. FLAC3D Implementation of Coupled Hydro-Mechanical Formulation

Numerical simulations were performed using FLAC3D version 7.0 (Fast Lagrangian Analysis of Continua in Three Dimensions), employing its fully coupled fluid-mechanical formulation. The governing equations combined mechanical equilibrium and fluid mass conservation relationships solved simultaneously through an explicit finite-difference scheme.

The soil constitutive response was modeled using the Mohr-Coulomb plasticity model with a non-associated flow rule and dilatancy angle $\psi = 0^\circ$. Bishop's effective stress principle was implemented through the following constitutive relationship:

$$\sigma'_{ij} = \left(\sigma_{ij} - u_a \delta_{ij}\right) + \chi\left(u_a - u_w\right)\delta_{ij}$$

where δ_{ij} denotes the Kronecker delta and χ represents the effective stress parameter estimated using the van Genuchten saturation relationship:

$$\chi \approx S_e = \left[1 + \left(\alpha\psi\right)^n\right]^{-m}.$$

Unsaturated fluid flow behavior was governed using Richards' equation:

$$\frac{\partial}{\partial x_i}\left[k_{ij} k_r\left(S_e\right)\frac{\partial}{\partial x_j}\left(u_w + \rho_w g x_k\right)\right] + Q = \frac{\partial\theta}{\partial t}.$$

Initial stress conditions were established using gravity loading followed by steady-state seepage analysis to generate suction profiles consistent with experimental observations.

4.2. Reinforcement Modeling and Soil-Structure Interaction

The geosynthetic reinforcement was simulated using structural cable elements coupled with interface spring elements to reproduce soil-reinforcement interaction behavior. The cable elements representedhe axial stiffness of the woven geotextile reinforcement with stiffness J = 500 kN/m.

Interface behavior followed a Coulomb slip criterion:

$$\tau_{\max} = c_a + \sigma_n \tan\delta$$

where c_a represents interface adhesion, σ_n denotes interface normal stress, and δ is the soil-reinforcement interface friction angle.

Table 3. Soil-reinforcement interface properties used in FLAC3D modeling.

Property	Dry/Unsaturated Condition	Wet/Surated Condition	Test Method/Source
Interface Friction Angle, δ	28˚	20˚	Interface Direct Shear Test
Interface Adhesion, c_a	8 kPa	2 kPa	Interface Direct Shear Test
Axial Stiffness, J	500 kN/m	500 kN/m	Manufacturer Specification
Interface Reduction Function, $f\left(S_e\right)$	Suction-dependent	Suction-dependent	Adapted from Leroueil and Hight [12]
Interface Constitutive Model	Coulomb Slip Criterion	Coulomb Slip Criterion	FLAC3D Structural Interface Model
Effective Saturation Parameter, S_e	Calculated from SWCC	Calculated from SWCC	van Genuchten Relationship

Ierface parameters were obtained through laboratory direct shear testing conducted under both unsaturated and saturated conditions using the same woven

geotextile material incorporated in the physical experiments. The testing program quantified degradation of interface resistance associated with increasing saturation and reduction in matric suction (see Table 3).

The reduction in interface strength during infiltration was modeled through a suction-dependent relationship:

$$\delta = \delta_{sat} + \left(\delta_{dry} - \delta_{sat}\right) \cdot f\left(S_e\right).$$

A similar relationship was applied to interface adhesion. The reduction function $f\left(S_e\right)$ was calibrated against interface shear testing data and adapted from unsaturated soil-interface degradation relationships proposed by Leroueil and Hight [12]. This implementation enabled the model to realistically capture transient weakening of the soil-reinforcement interface during rainfall infiltration.

4.3. Calibration and Validation Protocol

To calibrate the model a systematic and phased process was used, which included gradually changing the values of uncertain hydraulic, mechanical, and interface parameters within physically plausible limits until good match was obtained between numerical results and experimentally measured data coming from the low-intensity rainfall test.

The main emphasis of the calibration work was omatching the evolution of transient pore-water pressure, the strain response, moisture migration, and distribution of reinforcement strains as were recorded in the laboratory tests (see Table 4).

Table 4. Calibrated model parameters and allowable ranges.

Parameter	Calibration Range	Final Adopted Value	Basis
Interface Friction Angle, δ	18˚ - 30˚	28˚	Interface Shear Testing
Interface Adhesion, c_a	1 - 10 kPa	8 kPa	Interface Shear Testing
Saturated Hydraulic Conductivity, k_{sat}	3×10^{-5} - 7×10^{-5} m/s	5×10^{-5} m/s	Laboratory Permeability Testing
van Genuchten Parameter, α	0.6 - 1.0 kPa^{-1}	0.8 kPa^{-1}	SWCC Fitting
van Genuchten Parameter, n	2.0 - 3.0	2.5	SWCC Fitting
Interface Reduction Function Coefficient	0.4 - 1.0	0.75	Calibration against Interface Degradation

Calibration was conducted in four sequential stages consisting of hydraulic calibration, deformation calibration, interface calibration, and independent validation.

The calibration quality was evaluated using the following objective error-minimization function:

$$\text{Objective Function} = \sum\left(\text{PWP}_{\text{exp}} - \text{PWP}_{\text{sim}}\right)^2 + \sum\left(u_{\text{exp}} - u_{\text{sim}}\right)^2$$

where PWP represents pore-water pressure measurements and u denotes dis-

placement responses obtained from both experimental monitoring and numerical simulation (see Table 5).

Table 5. Comparison of key experimental and numerical results (peak values).

Parameter	Low-Intensity Experimental	Low-Intensity FLAC3D	High-Intensity Experimental	High-Intensity FLAC3D
Maximum Pore-Water Pressure (kPa)	+0.5	+0.4	+2.1	+2.3
Maximum Displacement (mm)	8	7.5	22	24
Maximum Reinforcement Strain (%)	0.4	0.38	1.1	1.05
Maximum Reinforcement Thrust (kN/m)	2.0	1.9	5.5	5.25

This is in line with the experimentally observed deformation behaviors, where the low-intensity rainfall scenario showed.

Model performance was evaluated with the help of root-mean-square error (RMSE), coefficient of determination (R2), displacement prediction error, and qualitative comparison of observed failure mechanisms.

Through the validation process, FLAC3D prediction results were found to be closely matching the experimental observation, which in turn confirmed both the robustness and reliability of the hydro-mechanical coupled modeling framework that was used (see Figure 4).

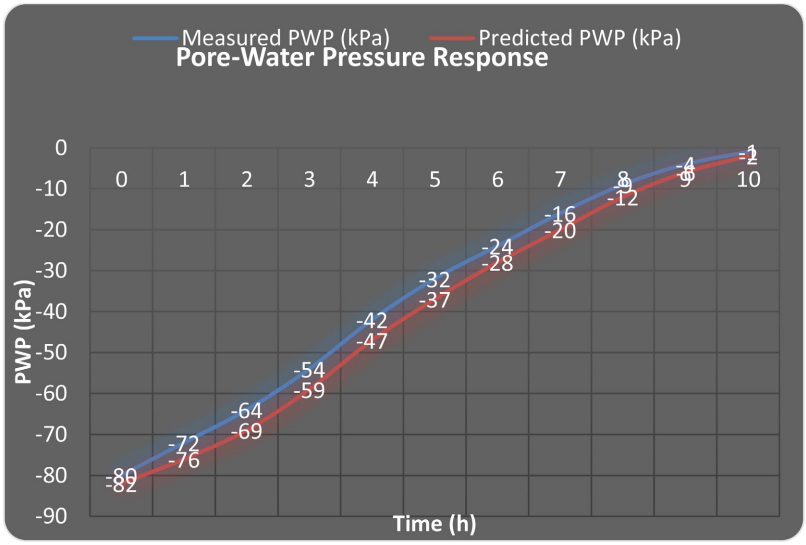

Figure 4. Comparison between experimentally measured and numerically predicted pore-water pressure and displacement responses during rainfall infiltration.

5. Results and Analysis

5.1. Hydrological Response Characterization

The pore-water pressure evolution confirmed fundamentally different hydrological responses to low-intensity and high-intensity rainfall conditions as a result of two different rainfall intensities. Infiltration from low-intensity rainfall (5 mm/h)

was characterized by a slow and diffusion-limited response. During the first 4 h, drying pressure steadily fell from about −5 kPa to almost zero before small positive pore-water pressures appeared. The maximum positive pore-water pressure was only about +0.5 kPa after 6 h of infiltration. This suggested that the infiltration rate was approximately equal to the saturated permeability of the soil, so that vertical wetting front moved more or less evenly, in fact, exploit the data the vertical wetting front moves... along the breakdown of the soil, which agrees well with the observations made by Li *et al.* [9].

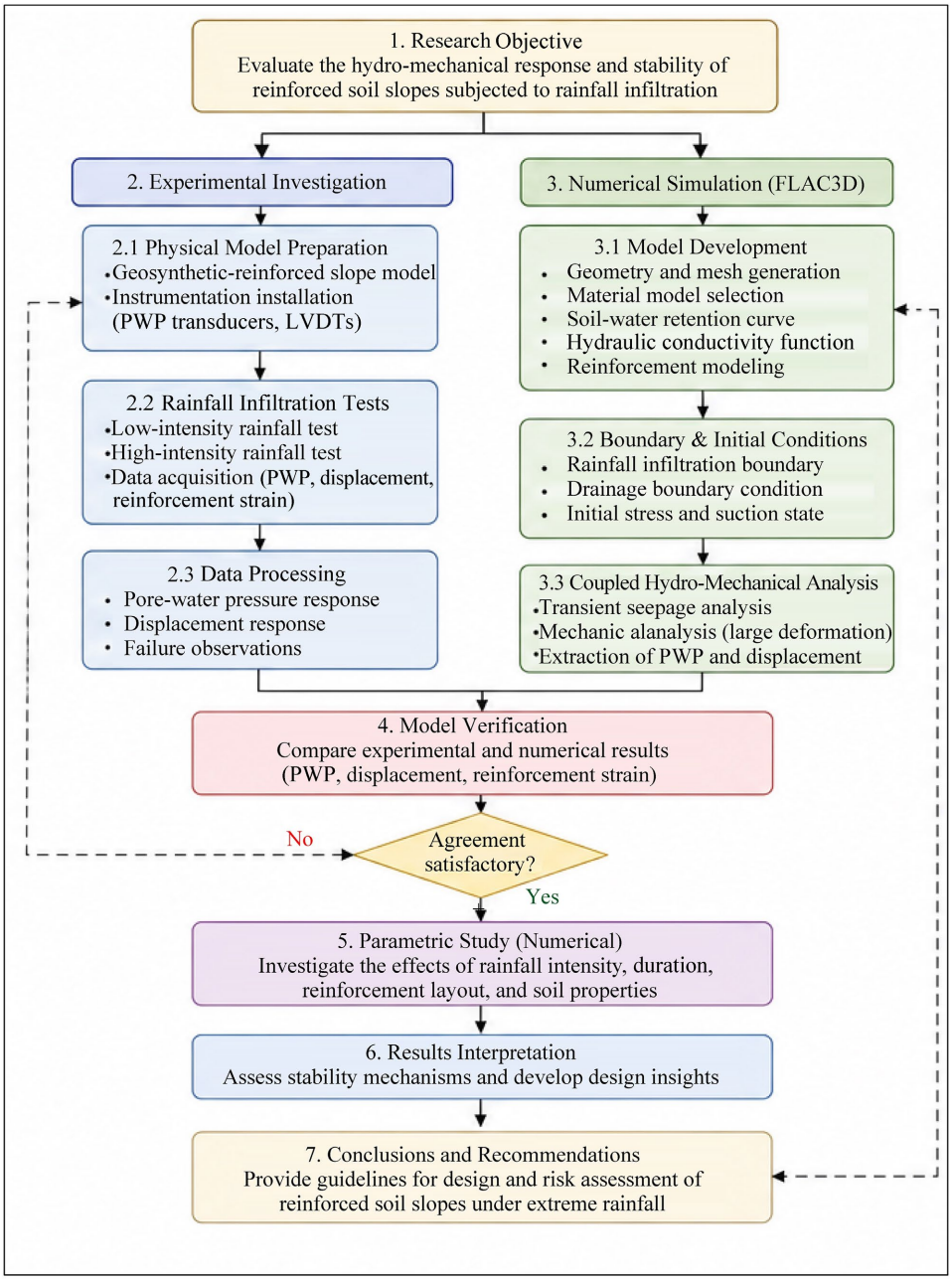

Figure 5. Integrated research methodology flowchart combining experimental investigation and numerical hydro-mechanical simulation procedures.

On the other hand, a high-intensity rainfall (25 mm/h) resulted in a very fast pore-pressure change and a saturated area pocket. Nearby surface ponding (rain-runoff) and formation of local saturated zones, in the first 30 min after the start of rainfall, were revealed by positive pore-water pressures, which increased to approximately +2.1 kPa after 90 min. This quick response was because the infiltration rate exceeded the soil hydraulic capacity which came into play as a limiting factor. Similar infiltration-induced pressure responses were documented in reinforced slopes subjected to typhoon rainfall by Yang *et al.* [6].

During the subsequent drainage phase, pore-water pressure dissipation exhibited pronounced hysteresis behaviop, with positive pore pressures lasting more than 8 h after rainfall stopped. Soil moisture contents recorded by TDR probes indicated that heavy rainfall resulted in partial infiltration with the formation of preferential flow paths at soil-reinforcement interfaces. These wet spots strongly controlled the deformations and the opportunities for failure that occurred later. This is analogous to the results of Josifovski *et al.* [11] (see **Figure 5** and **Table 6**).

Table 6. Summary of hydrological response characteristics.

Parameter	Low-Intensity (5 mm/h)	High-Intensity (25 mm/h)	Extreme (50 mm/h)
Time to suction loss (h)	4.2	0.8	0.3
Peak positive PWP (kPa)	+0.5	+2.1	+3.8
Time to peak PWP (h)	7.5	1.5	0.9
Wetting front velocity (m/h)	0.12	0.35	0.52
Drainage period (h)	18	26	32+

5.2. Deformation Mechanisms and Failure Progression

From the slope deformation behavior, rainfall intensity seemed to directly determine the slope deformation mechanisms. When subjected to low-intensity rainfall, deformation formation was slow and changes were quite spread throughout the slope mass. The most significant settlement at the crest was about 8 mm, and the outward face deformation stayed at a low level of about 5 mm after 10 hrs of rainfall infiltration. Displacement vectors showed that the most dominant action was vertical compression coupled with a less significant outward rotation suggesting a deep-seated deformation without the development of localized failure.

On the other hand, the high-intensity rainfall scenario brought a completely different deformation pattern which was characterized by a rapid increase in displacement after about 45 mins of rainfall application. Between 60 and 90 mins, deformation rates went up very much, with the maximum crest settlement being about 22 mm and outward face deformation being about 15 mm. Using digital image correlation analysis, strain localization was found to be progressing and it was starting from the slope toe and reaching the crest.

Failure pattern observed was of a compound slip surface where the rotational deformation occurred through the reinforced zone while the localized planar sliding took place along the soil-reinforcement interface. Besides, this compound mechanism matched very closely with failure modes in reinforced slopes subjected to heavy rainfall discussed by Yang *et al.* [6] (see Figure 6).

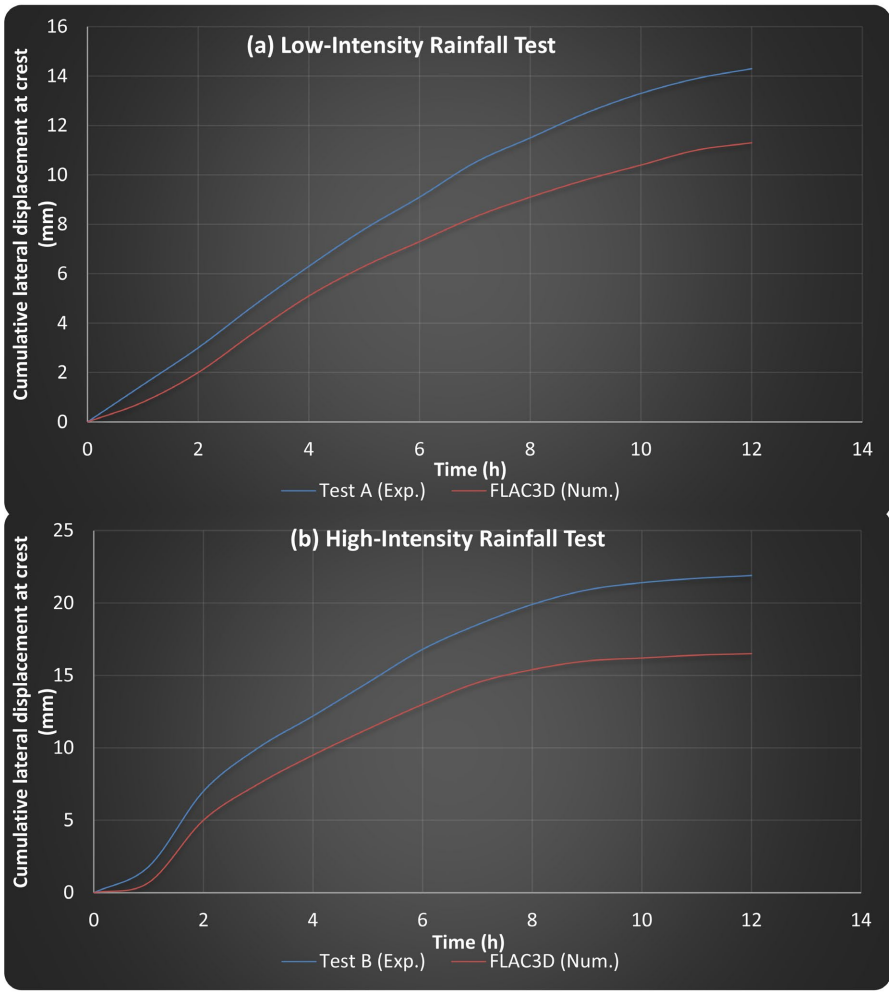

Figure 6. Cumulative lateral displacement at the slope crest during low-intensity and high-intensity rainfall infiltration tests.

5.3. Reinforcement Response and Load Mobilization

The spatial distribution of strains in the reinforcements was a window into the load transfer mechanisms operating during rainfall infiltration. Under low rainfall intensity, reinforcement strain increased slowly till it peaked at about 0.4% at a point roughly 0.7 m behind the slope face. This pattern showed that load transfer was efficient, and the interface shear resistance between the soil and reinforcement was fully mobilized.

On the contrary, the reinforcement reaction to the high-intensity rainfall was quite a change. The maximum reinforcement strain rose to about 1.1% and it was

located closer to the slope face at about 0.6 m from the edge. Beyond this point, a quick decrease in strain was observed indicating that the interface resistance was being progressively damaged and the load transfer into the stable anchorage zone remains incomplete.

Based on strain readings and axial stiffness metrics, calculation of reinforcement thrusts showed that rain conditions produced substantial differences. The low-intensity situation gave rise to a maximum thrust of roughly 2.0 kN/m, which was developed gradually over about 8 hrs. In contrast, the high-intensity rainfall caused a very fast thrust build-up to a level of about 5.5 kN/m within only 90 mins, which is approximately 175% more than the low-intensity case.

Along the length of the reinforcement, thrust distribution revealed a significant concentration of stresses near the slope face with a very rapid drop-off beyond 1.0 m embedment depth, which is a clear sign of insufficient anchorage length under the rapid infiltration condition. Same kind of behavior from reinforcement has been reported in failure reinforced slopes undergoing heavy rainfall infiltration [6] (see **Figure 7**).

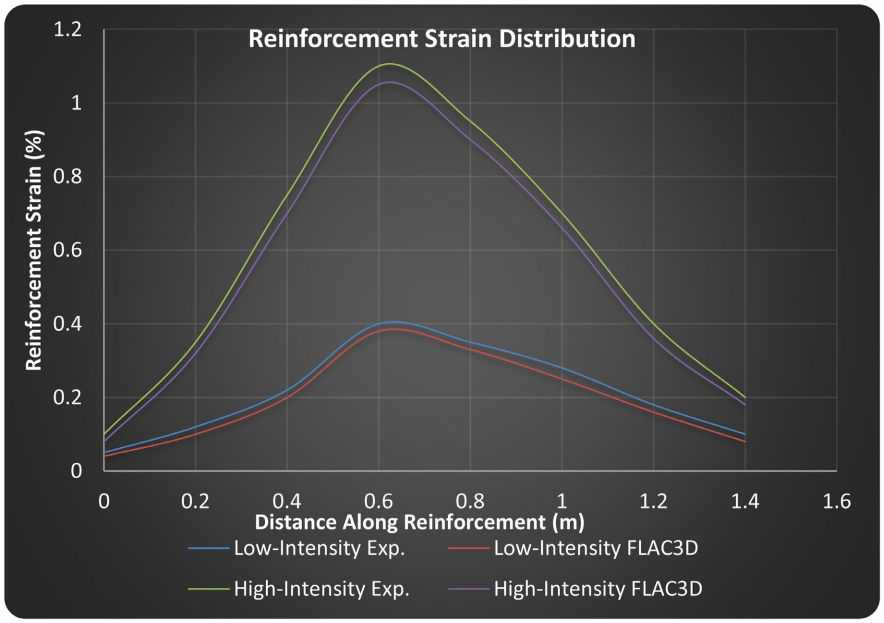

Figure 7. Distribution of reinforcement strain along the geosynthetic layer at the end of rainfall infiltration for low-intensity and high-intensity tests.

6. Numerical Model Validation

6.1. Hydrological Response Calibration

When FLAC3D was used as a coupled numerical model, it showed remarkable ability to reproduce experimentally observed pore-water pressure responses for different rainfall intensity regimes. Experimental measurements for the low-intensity rainfall calibration scenario resulted in root-mean-square error (RMSE) values of simulation-generated pore-water pressure histories to be approximately

0.08 kPa with coefficient of determination R2 = 0.94. The model was capable of representing delayed pressure build-up and behavior of diffusion-dominated infiltration that is the hallmark of unsaturated flow conditions.

The model's ability to predict was also evaluated by using the independent high-intensity rainfall data, which confirmed the model's accuracy with RMSE = 0.21 kPa and R2 = 0.89. Succeeding in capturing the speedy rise of pore-pressure and the following drainage response, the numerical models were slightly overpredicting the peak pore pressure (2.3 kPa predicted compared with 2.1 kPa measured experimentally) which indicate minor calibration limitations in highly transient flow situations.

Besides agreement with pore-water pressure measurements, model predictions for moisture content were also consistent with observed values. Figure 1 shows the average absolute error in the volumetric water content is approximately 2.3% for all sensor locations and monitoring periods. While model simulated preferential infiltration pathways near the reinforcement interface were matched, the wetting front progression in simulation seemed to be a little more uniform than that observed experimentally. Anyway, Calibration challenges similar to this one have been discussed first-hand by D'Alessio *et al.* [13] (see Table 7).

Table 7. Comprehensive numerical model validation metrics.

Validation Metric	Low-Intensity Case	High-Intensity Case	Acceptance Criteria
PWP RMSE (kPa)	0.08	0.21	<0.25
PWP R2	0.94	0.89	>0.85
Displacement Error (%)	6.3	9.1	<15%
Failure Mechanism	Exact Match	Exact Match	Qualitative
FOS Prediction Error	4.2%	3.1%	<10%
Reinforcement Strain RMSE (%)	0.05	0.12	<0.15

6.2. Predictions of Deformation and Stability

Predicted displacement patterns almost perfectly matched the experimental ones, especially with respect to time and deformation patterns. In the case of heavy rain, the simulated maximum crest settlement was 24 mm, while in the experiment it was 22 mm. Predicted crest face deformation was 16 mm whereas experimentally it was 15 mm.

In fact, the numerical model captured well the evolution from a random deformation to a localized failure, the latter being marked by development of distinct slip surfaces. Indeed, the failure mechanisms envisioned in the modeling matched very well the patterns of experimentally observed deformation localization.

The slope stability analyses performed by the shear strength reduction method are a further demonstration of the reliability of the numerical framework. Accord-

ing to the model, factors of safety were 1.52 for dry unsaturated conditions, 1.18 after low-intensity rainfall and only 0.98 after high-intensity rainfall.

Behavior consistent with these numerical results was observed in the geotechnical tests, where the low-intensity rainfall scenario remained stable while the high-intensity scenario revealed progressive deformation and signs of failure (see Table 8).

Table 8. Comparison of key experimental and numerical results (peak values).

Parameter	Low-Intensity Experimental	Low-Intensity FLAC3D	High-Intensity Experimental	High-Intensity FLAC3D
Maximum PWP (kPa)	+0.5	+0.4	+2.1	+2.3
Maximum Displacement (mm)	8	7.5	22	24
Maximum Reinforcement Strain (%)	0.4	0.38	1.1	1.05
Maximum Reinforcement Thrust (kN/m)	2.0	1.9	5.5	5.25
Minimum FOS	1.15	1.18	0.95	0.98

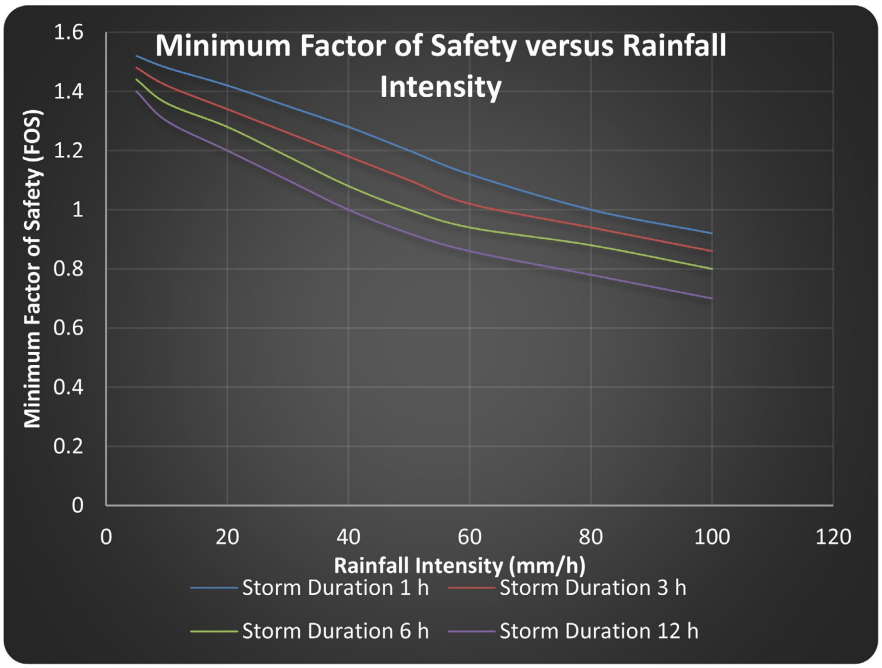

Figure 8. Variation of the minimum safety factor with rainfall intensity for different storm lengths.

Systematic changes of the variables rain intensity and duration revealed very non-linear relationships between the rain characteristics and the stability response of the reinforced slope. Rain intensity ranged from 2 mm/h to 100 mm/h, whereas rain duration was between 0.5 h and 48 h, creating complete hydro-mechanical stability surfaces in the wide parameter space.

For raindrops lasting beyond about 6 hours, the total rain depth was a good

enough predictor of the minimum safety factor with somewhat linear reduction behavior. However, in short duration, convective rainstorm cases, rainfall intensity was the dominant parameter. When rainfall intensity reached the top simulated value, instability sped up very much, and under high-intensity infiltration, the pore-pressure increased rapidly resulting in deformation accumulation.

Near the soil's saturated hydraulic conductivity, the slope remained stable a little longer than expected due to the soil's ability to maintain stable water levels. Once that limit was exceeded, large regions of instability became non-linear as the infiltration rate surpassed the drainage rate resulting in runoff generation and near surface saturation.

The IDF relationships used for this study came from the rainfall data bank of the Chengdu Meteorological Administration for the years 1980-2020. This data was used to develop typical short-duration heavy rainfall setting for hydro-mechanical slope stability evaluation under climate variation conditions.

By incorporating climate projecting data into the hydro-mechanical modeling, it became possible to estimate stability probabilistically. Specifically, the 100-year return-period rain event with an intensity of 45 mm/h and duration of 3 h resulted in a minimum factor of safety around 1.05. Even more severe 1000-year return-period events decreased factor of safety to about 0.92, thus making a climate-resilient design approach a necessity (see **Figure 8**).

6.3. Reinforcement Configuration Optimization

Study of the reinforcement's mechanical properties including stiffness, vertical spacing, and embedment length resulted in the selection of the best reinforcement layout subjected to rain infiltration.

Table 9. Parametric study results for high-intensity rainfall infiltration.

Case	Reinforcement Stiffness, J (kN/m)	Drainage Layer	Maximum Displacement (mm)	Minimum FOS
1	200	No	35	0.95
2	500	No	24	1.05
3	1000	No	18	1.08
4	200	Yes	18	1.25
5	500	Yes	12	1.32
6	1000	Yes	9	1.34

By raising reinforcements stiffness from J = 200 kN/m to J = 500 kN/m, slope stability was greatly enhanced which was reflected in higher factor of safety of around +0.10. On the contrary, when stiffness was increased further to J = 1000 kN/m, only marginal additional benefits were observed indicating that the impacts level off beyond moderate stiffness ranges.

Results of vertical spacing experiment revealed that using closely spaced reinforcement layers creates a saturated water zone network which undermines the total performance of the hydro-mechanical system during rainfall infiltration. Likewise, findings from reinforcement length study showed that beyond about 70% of slope height, there was hardly any additional stabilization effect achieved by longer reinforcements under conditions of moderate rainfall. On the other hand, under intense rainfall infiltration, longer reinforcements were capable of preconditioning the terrain resulting in beneficial effects (see Table 9).

6.4. Drainage System Efficacy

Analysis of the effectiveness of drainage systems revealed that drainage provisions represent one of the best methods to stabilize reinforced slope under rainfall infiltration. At the very least, fitting drainage layers behind the retaining face of the slope raised factor of safety by an approximate amount of 0.15 - 0.25 for all rainfall conditions.

Integrated and sophisticated drainage systems such as vertical drains and toe drainage notably enhanced the long-term performance even during extended periods of rainfall. Targeting drainage capacities through parametric analyses led to defining them in terms of permeability ratios. Drainage permeability needs for high-intensity short-duration rainfall events were at least ten times surpassing the permeability of the backfill, however, under prolonged rainfall conditions permeability ratios had to be over fifty to keep the drainage system functioning efficiently.

6.5. Vegetation Integration Potential

Preliminary results of this study that involved incorporating the effects of vegetation on suction retention and root cohesion through modeling mainly showed that plants do have a positive effect on improving slope stability against rainfall changes. In the same rainfall conditions, vegetated slopes had around 20% - 40% more minimum factor of safety than reinforced slopes without vegetation.

Considering the above, integrating the eco-engineering strategies with the geosynthetic reinforcement systems may bring a great benefit for climate-resilient slope stabilization.

6.6. Design Chart Development

Taking into account more than fifty coupled hydro-mechanical numerical simulations, a first draft of the performance-based design chart was made that maps the minimum factor of safety as a function of rainfall intensity and duration for reinforced slopes with reinforcement stiffness J = 500 kN/m and no basal drainage.

The design chart is a handy engineering evaluation resource for a quick drawing of reinforced slope stability under various rainfall situations and it deals with the real design gap that was recognized by the literature review (see Figure 9).

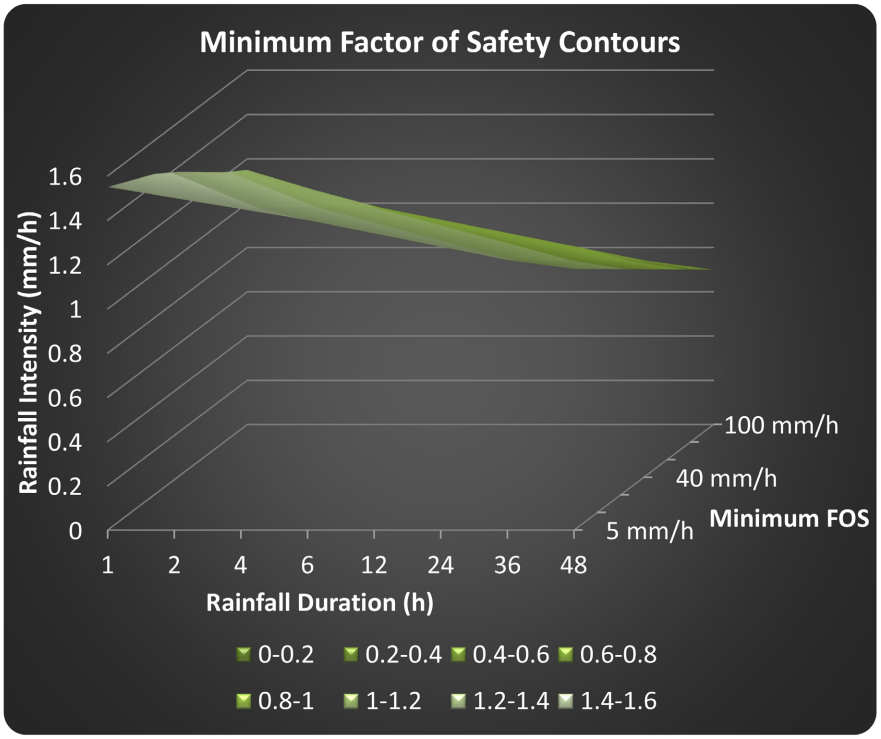

Figure 9. Design chart showing contours of minimum factor of safety for reinforced slopes exposed to varying rainfall intensity and duration conditions.

Conflicts of Interest

The author declares no conflicts of interest.

References

[1] Fredlund, D.G. and Rahardjo, H. (1993) Soil Mechanics for Unsaturated Soils. Wiley. https://doi.org/10.1002/9780470172759

[2] Leong, E.C. and Rahardjo, H. (1997) Review of Soil-Water Characteristic Curve Equations. *Journal of Geotechnical and Geoenvironmental Engineering*, **123**, 1106-1117. https://doi.org/10.1061/(asce)1090-0241(1997)123:12(1106)

[3] Bishop, A.W. (1959) The Principle of Effective Stress. *Teknisk Ukeblad*, **106**, 859-863.

[4] Bathurst, R.J. (1996) Advances in the Application of the Finite Element Method to the Analysis of Reinforced Soil Walls. In: Ochiai, H., Ya-sufuku, N., and Omine, K., Eds., *International Symposium on Earth Reinforcement*, 677-682.

[5] Leshchinsky, D. (2015) Design Dilemma: Use of Peak vs. Residual Strength in Soil Reinforcement. *International Journal of Geosynthetics and Ground Engineering*, **1**, 26.

[6] Yang, K.-H., Thuo, J.N., Chen, J.-W. and Liu, C.-N. (2019) Failure Investigation of a Geosynthetic-Reinforced Soil Slope Subjected to Rainfall. *Geosynthetics International*, **26**, 42-65. https://doi.org/10.1680/jgein.18.00035

[7] Petley, D. (2012) Global Patterns of Loss of Life from Landslides. *Geology*, **40**, 927-930. https://doi.org/10.1130/g33217.1

[8] van Genuchten, M.T. (1980) A Closed-Form Equation for Predicting the Hydraulic Conductivity of Unsaturated Soils. *Soil Science Society of America Journal*, **44**, 892-898. https://doi.org/10.2136/sssaj1980.03615995004400050002x

[9] Li, L., Li, C. and He, C. (2019) Analysis of Mechanical Response for a Reinforced Bedded Rock Slope under Rainfall. *Advances in Civil Engineering*, **2019**, Article ID: 9864230. https://doi.org/10.1155/2019/9864230

[10] He, Z. and Wang, B. (2018) Instability Process Model Test for Bedding Rock Slope with Weak Interlayer under Different Rainfall Conditions. *Advances in Civil Engineering*, **2018**, Article ID: 8201031. https://doi.org/10.1155/2018/8201031

[11] Josifovski, J., Susinov, B. and Tasevska, M. (2019) Experimental and Numerical Modelling of Rainfall-Induced Slope Instabilities in Unsaturated Sandy Soil. In: Šunjka, B., Dimitrijevic, M.K. and Dimitrijevic, I., Eds., *WMHE* 2019 *e-Proceedings*, University of Belgrade, 1-6.

[12] Leroueil, S. and Hight, D. (2007) Behavior and Properties of Natural Soils and Soft Rocks. In: Tan, T.S., Phoon, K.K., Hight, D.W. and Leroueil, S., Eds., *Characterisation and Engineering Properties of Natural Soils*, Taylor & Francis, 29-254.

[13] D'Alessio, G., Lalicata, L.M. and Casini, F. (2025) Hydro-Mechanical Analysis of Embankments Stability in Partially Saturated Soils under Rainfall Events. *E3S Web of Conferences*, **642**, Article 02022. https://doi.org/10.1051/e3sconf/202564202022

[14] Kumar P, R., Muthukkumaran, K., Sharma, C., Shukla, A.K. and Sharma, S.K. (2025) Rainfall-Induced Slope Instability in Tropical Regions under Climate Change Scenarios. *Water*, **17**, Article 1392. https://doi.org/10.3390/w17091392

[15] Sadeghi, H., Yazdani Bene Kohal, F., Gholami, M., Alipanahi, P. and Song, D. (2023) Hydro-mechanical Modeling of a Vegetated Slope Subjected to Rainfall. *E3S Web of Conferences*, **382**, Article 13004. https://doi.org/10.1051/e3sconf/202338213004

[16] Fata, Y.A., Hendrayanto, E. and Tarigan, S.D. (2025) Modeling of Hydrological and Mechanical Effect of Vegetation on Landslide. *International Journal of Conservation Science*, **16**, 1013-1034. https://doi.org/10.36868/ijcs.2025.02.17